Composite Structures 330 (2024) 117813

Contents lists available at ScienceDirect

Composite Structures

journal homepage: www.elsevier.com/locate/compstruct

Experimental characterization of a Polymer Metal Hybrid (PMH) automotive structure under quasi-static, creep, and impact loading

A. Canegrati [a], A. Bernasconi [a,*], L.M. Martulli [a], P. Barriga [a], G. Previati [a], D. Fiumarella [b], A. Scattina [b], E. Spini [c], G. Belingardi [b], G. Mastinu [a]

[a] Department of Mechanical Engineering, Politecnico di Milano, Milano, Italy
[b] DIMEAS, Politecnico di Torino, Torino, Italy
[c] RadiciGroup High Performance Polymers, Chignolo d'Isola BG, Italy

ARTICLE INFO

Keywords:
Composite suspension arm
Polymer Metal Hybrid technology
Experimental tests

ABSTRACT

A feasibility study on a short fibre reinforced Polymer Metal Hybrid (PMH) solution of a car's suspension control arm has been conducted through a simplified demonstrator, representative of the most critical portion of this component. It was injection moulded in two versions: an all composite one and a PMH version, in which the short fibre reinforced composite was over-moulded on to an aluminium insert. The demonstrator underwent quasi-static, creep and impact tests to simulate most of the loading conditions experienced by a suspension arm during its lifetime. The mechanical behaviours of the two demonstrator versions were compared to highlight the differences introduced by the proposed novel PMH solution. In particular, the ductile metal insert ensured the compliance of the PMH demonstrators with the automotive specific safety requirement of avoiding the complete separation at failure, which was successfully obtained in all testing conditions.

1. Introduction

Complying with the current regulations concerning emissions reduction and meeting the growing demand for sustainable products are among the greatest challenges that car manufacturers are facing in our time. The achievement of these goals calls for a further vehicle mass reduction, paying special attention to the design of durable components using lightweight recyclable materials.

The reduction of vehicle weight by replacing metals with high-performance polymers has been underway for several decades, and it also applies to structural components such as engine mounts, air intake manifolds, engine oil pans, valve covers, body in white inserts, front ends (PMH solution), etc. However, for safety–critical components such as brake pedals, suspension arms, etc., the use of metals is still predominant [1].

In this framework, the suspension system draws particular attention of the designers because it builds up to the 25 % of the whole mass of a vehicle [2]. Beside the impact on the overall mass of the vehicle, a lightweight suspension system would bring benefits in car handling and occupants' comfort, thanks to the reduction of the unsprung masses [2,3]. Although over the last two decades suspension control arms have been mainly produced from steel, aluminium castings, and ductile iron casting [4], several composite suspension arms have been proposed in literature, using continuous fibre reinforced thermosetting polymers [2,4–7].

Carello et.al [5] developed an extended feasibility study for engineering of a suspension upper control arm made by Carbon Fibre Reinforced Polymer (CFRP). The component was designed with composite optimization methodology, to take advantage of the CFRP properties. Although no weight reduction was achieved, an average increase of 78 % in stiffness was obtained as compared to other lightweight materials. Overall, the car performance was thus significantly improved by adopting CFRP solution.

Kim et al. [6] designed a suspension lower arm for automotive applications made of high strength carbon/epoxy composite. Through stacking angles optimization, the composite lower arm displayed two times higher stiffness and buckling strength than a conventional steel lower arm, being 50 % lighter.

Banks [7] designed a composite rear suspension knuckle/tie blade consisting of UD prepreg (epoxy resin), SMC (vinylester resin) carbon fibre and a steel insert. This solution ensured a weight reduction of 35 % compared to serial produced components. The use of chopped strand

* Corresponding author.
E-mail address: andrea.bernasconi@polimi.it (A. Bernasconi).

https://doi.org/10.1016/j.compstruct.2023.117813
Received 19 July 2023; Received in revised form 25 November 2023; Accepted 13 December 2023
Available online 15 December 2023

mats was also proposed for developing suspension arms in [8].

Despite the outstanding stiffness and strength to weight ratios offered by CFRPs, they are usually prone to brittle and catastrophic failure [9]. Ductile failure mechanisms and residual integrity of the components are known to be binding requirements for the automotive industry, concerning safety-relevant components. Therefore, the undesired failure mode of CFRPs, in addition to their high cost and their end life disposal, contributed to restrict their spreading across the automotive sector.

Polymer Metal Hybrid (PMH) technology, instead, allows the design of lightweight structures with improved mechanical behaviour. PMH design combines the high ductility of metals and the high specific mechanical properties of polymer-based composites. For example, adding fibre reinforced polymer layers can improve the bending behaviour of metal beams [10] prevent premature buckling failure [11] or improve its crashworthiness [12,13].

An attempt to develop a multi-material lower control arm of a McPherson suspension system was carried out by Messana et al. [3]. The mass of an existing steel arm was reduced by applying a hybrid technology. The thickness of the component was diminished and a CFRP tailored cover was added. This hybrid solution showed a stiffness comparable with the original arm, achieving a 23 % of mass reduction.

However, the use of composites poses the challenge of complying with regulations about recycling of structures, which call for the separation of metals and composites [14]. The use of thermosetting matrices and continuous fibres for the manufacturing of suspension components, can make recovery and separation more difficult. Conversely, the use of thermoplastic-based fibre reinforced polymers appears to make separation easier [15], e.g. by grinding, gravimetric separation, remelting of the polymer.

Several applications of injection moulded, short fibre reinforced polymer parts can be found in the automotive industry, including load bearing applications, e.g. clutch pedals, engine mounts or torque rods. However, for many structural components, especially those classified as safety-related, the use of engineering polymers is still marginal. Some components, like suspension arms, have additional design specifications, namely no separation after failure, that prevent form the adoption of relatively brittle materials like Short Fibre Reinforced Polymers (SFRP) only, and suggest the adoption of a PMH solution. For the manufacturing of the short fibre reinforced PMH components, the fibre reinforced thermoplastic polymer is over-moulded onto a thin metallic component. An in-depth analysis of the contribution of injection moulded ribs on the mechanical performance of a channel beam-like structure [16] demonstrated that the ribs can increase the load-bearing capacity of the structure, leading to reduced weight compared to a closed box section. The feasibility of this type of construction has been thoroughly investigated, with special focus on the adhesion between the metallic and polymeric parts [16–20]. Generally, the quality and the strength of the adhesion depend on the surface topography and chemistry of the metal (resulting from the surface treatment to which the metal undergoes), as well as on the viscosity of the melt polymeric compound, which is given by the injection moulding parameters as temperature and pressure. Several studies have been conducted on the direct-adhesion injection overmoulded polymer-metal joints [21]; for a comprehensive review of the state of the art the reader can refer to [22].

In the automotive sector, the AUDI hybrid front-end [23] was one of the first and most popular application of PMH [24–26]. More recently, Mercedes and partners developed a PMH front-end module for the B-Class car, in which a closed tube-shaped aluminum piece is overmoulded with glass-fibre reinforced nylon 6 (PA6-GF) [22]. The Trelleborg Group proposed a hybrid brake pedal, in which a metal insert is overmoulded with glass fibre reinforced plastic [22]. A PMH engine cradle was proposed [27], and optimized topologically by multi material topological optimization [28] and by an integrated finite element/artificial neural network multi-objective optimization approach [29]. PHM structures with continuous fibre reinforced thermoplastic sheets for energy absorbing applications were also proposed [30].

The goal of the present work is to demonstrate the feasibility of a short fibre reinforced PMH solution for the suspension system of a car. In this article, we present a simplified demonstrator, designed to comply with the design requirements of a McPherson suspension arm. The demonstrator is a tapered I-beam-like structure that replicates in a simplified manner the portion of a suspension arm that undergoes bending, as in the usual operation of the suspension during vehicle riding. The idea is shown schematically in Fig. 1.

The PMH demonstrator consists of an outer short fibre reinforced polymeric shell which embodies a metallic insert. Such a hybrid solution was specifically designed so that the composite shell is its actual load bearing component. Therefore, the mechanical properties of the PMH demonstrator, such as stiffness and strength, are those exclusively provided by the composite shell itself. This implies that a brittle failure is expected for the composite shell, most likely resulting in the complete separation in two halves of the demonstrator in a catastrophic fashion, unless the metal insert is used. Thus, the metal insert is intended to be the structural elements which preserve the residual integrity of the PMH demonstrator after failure of the composite shell.

The preliminary design of the PMH demonstrator was supported by quasi-static Finite Element Modelling (FEM) numerical simulations. Advanced methods based on state-of-the-art solutions available in commercial software packages were employed, to account for the anisotropy, the variability of the fibre orientation induced by the manufacturing process, and the non-linearity of the quasi-static behaviour of the material.

The demonstrator was manufactured by injection moulding and tested statically and dynamically to simulate the everyday working conditions of a suspension control arm. A version of the demonstrator without the metallic insert was also manufactured and tested. The mechanical behaviour of the two demonstrator versions were thus compared and the effect of the internal reinforcement of the PMH version discussed.

To the best of the authors' knowledge, no short fibres reinforced PMH solutions for suspension arm proposed in the literature adopt such a design concept nor have been tested for a feasibility assessment.

2. Materials and methods

2.1. Demonstrators design and manufacturing

The portion of the car's suspension control arm, replicated by the demonstrator, can be treated as a cantilever beam subjected to a bending load. Its wheel-side end is free to deflect, while the rigid connection of its chassis-side end is fixed to the remaining part of the suspension lower arm, as shown in Fig. 1. Because of the complexity of the structure, in a real testing condition it is challenging to constrain the demonstrator's chassis-side end to simulate the material continuity. Moreover, due to the presence of elastic bushings in the suspension arm, a rigid clamping would not be realistic. Therefore, the demonstrator, was mirrored about its chassis-side vertical plane, to test it in Three Point Bending (TPB) mode, as schematically shown in Fig. 2. This testing configuration allows the mid span deflection of the structure to be assumed equal to the end tip deflection of the structure in the cantilever beam model.

The PMH demonstrator consisted of two components: the main structure, made of a 50 % by weight Short Glass Fibre Reinforced special polyamide-66 (SGFR-PA66), provided by RadiciGroup High Performance Polymers under the tradename of RADISTRONG A RV 500 W and a 6061-T6 aluminium insert, embodied in the main structure. The composite main structure is the load bearing element. It must be effectively designed to withstand the same type of loading as the car's suspension control arm is subjected during its working lifetime. The aluminium insert, instead, was meant to meet the specific requirement of avoiding the complete separation of the PMH demonstrator at failure. The CAD models of the PMH demonstrator, the drawings of the

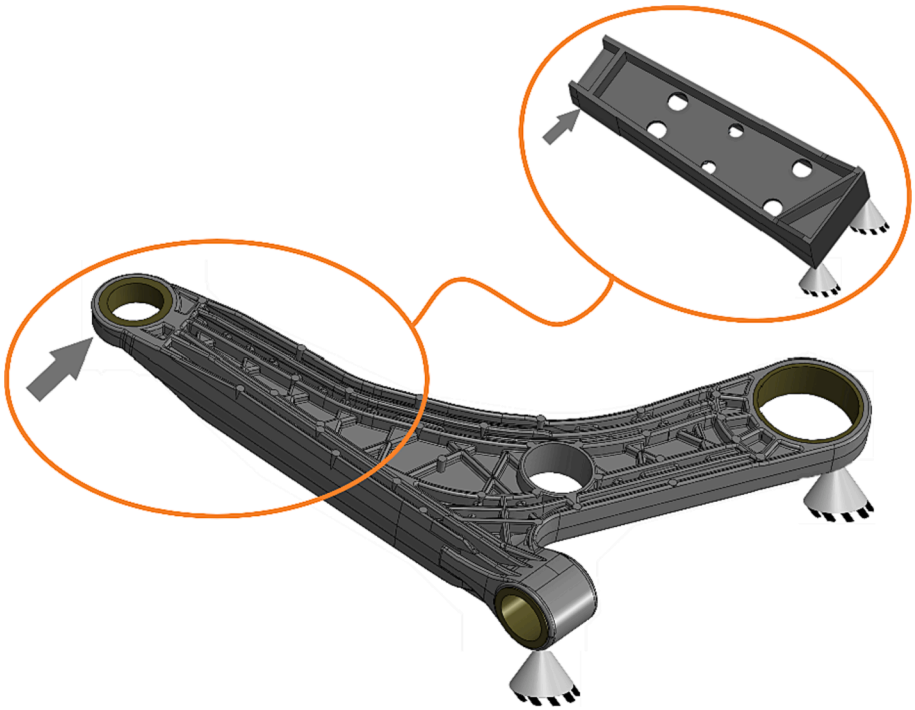

Fig. 1. Geometry simplification from the real suspension arm to the analysed demonstrator. Loading conditions of the control arm are also reported.

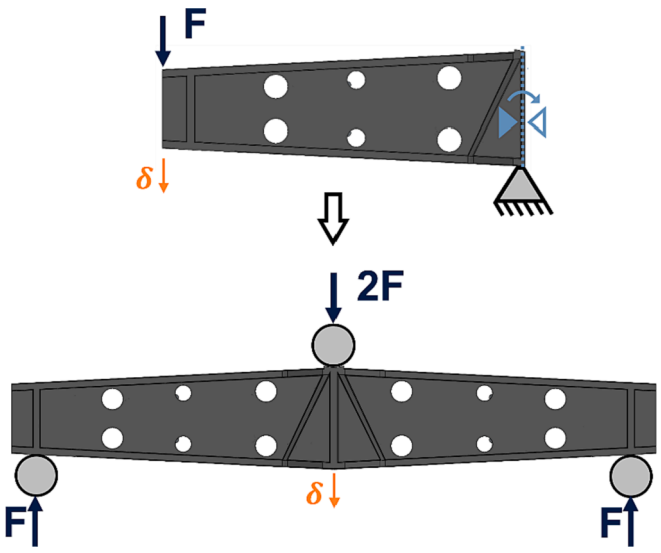

Fig. 2. Schematic representation of the demonstrator mirroring for three-point bending test, Forces (F) and displacements (δ) are highlighted.

composite main structure and of the aluminium insert are shown in Fig. 3, along with their dimensions.

To assess the crucial role of the aluminium insert in preventing the complete separation of the structure at failure, demonstrators without the insert (here after referred to as "polymeric demonstrator") were also fabricated and tested. The polymeric demonstrator thus consisted of the composite main structure only, reported in Fig. 3.b.

Both demonstrator versions were injection moulded. A steel mould was manufactured specifically for this component. In the case of the PMH demonstrator, the insert, laser cut from an aluminium sheet, was first placed in the mould, then the short glass fibre reinforced polyamide was over-moulded on to it. The injection moulding of the SGFR-PA66 was performed on an Engel 120 T hydraulic injection moulding machine with a screw diameter of 40 mm. The temperature of the melt was 280 °C, while that of the mould was of 110 °C.

The aluminium insert did not undergo any surface treatment but solvent cleaning before the injection process. Since the insert is extracted from rolled aluminium sheet, it displays a surface roughness of 0.13 μm and of 0.46 μm. in the rolling and transverse directions, respectively. It displays a truss-like structure which allows the component to be light and stiff. The holes were created on the insert to keep it in place under the action of pressure exerted by the flow of molten material during the injection process. Top and bottom flanges of the composite main structure were designed with draft angles to facilitate the extraction of the demonstrator from the mould at the end of the solidification.

Flat surfaces were located on the demonstrator's bottom flanges where the contact between the demonstrator and the fixed supports of the TPB rig develops. This design choice increases the contact area avoiding the development of a single point contact, resulting from the design of the flanges with draft angles.

A cylindrical housing for the TPB loading cylinder was created at mid-span of the demonstrator's top flange. This maximises the contact area between the loading cylinder and the demonstrator, reducing the contact pressure.

Vertical ribs were introduced in the main structure. They are located at the contact sections between the demonstrator and both the fixed supports and the loading edge. The use of ribs increases the stiffness of these sections that are subjected to high shear forces during the TPB test. Moreover, oblique reinforcement ribs, running from the contact region with the loading cylinder to the lower flanges, were also designed to induce failure at the end of the oblique rib in the lower flange.

An injection moulding simulation was performed using the Autodesk Moldflow 2019 software [31] to evaluate the Fibre Orientation Distribution (FOD) across the PMH demonstrator (adopting the Reduced Strain Closure model). On the demonstrator's upper flanges, two injection gates, symmetrically located about its mid-span vertical axis, were used to perform the simulation of the injection process. Simulation results are expressed in terms of the 2nd order orientation tensor [32].

Fig. 4 showcases the local maximum eigenvalue of the orientation tensor along with the locations of the injection gates used. High values

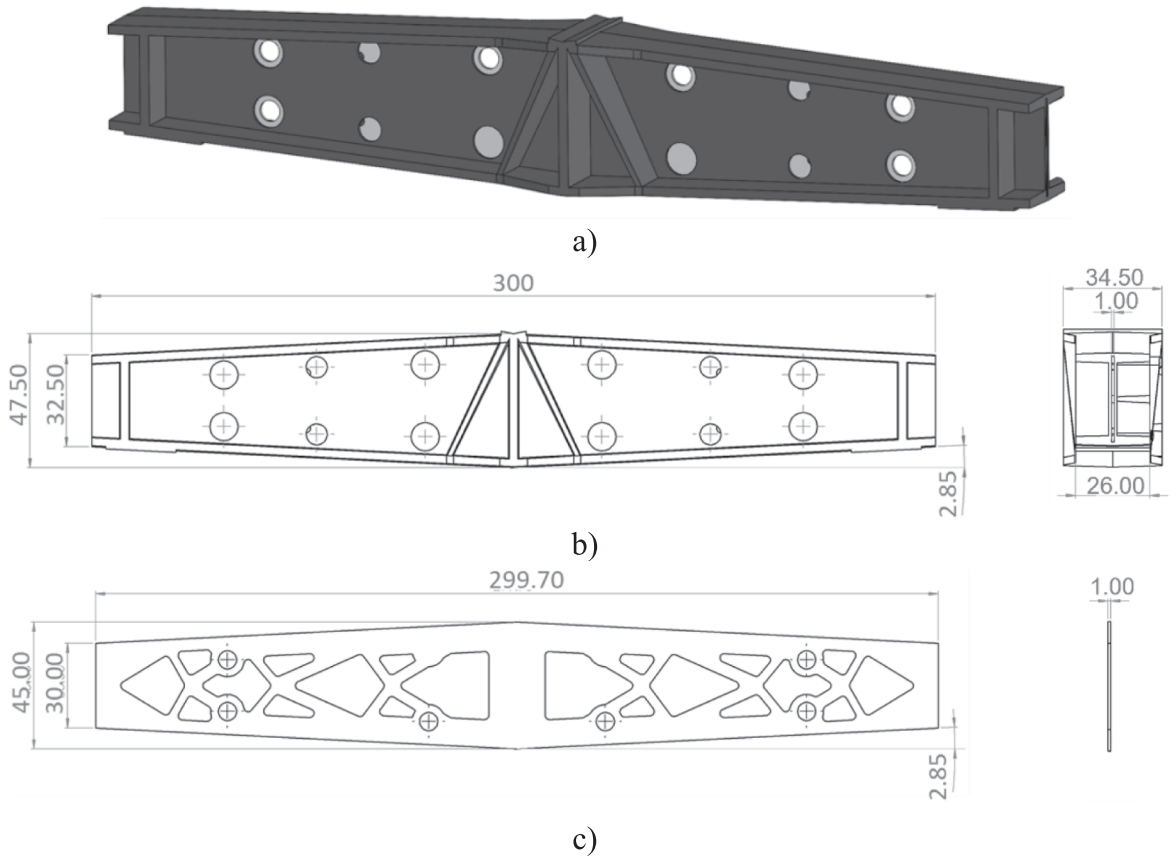

Fig. 3. A) CAD model of the PMH demonstrator and drawings of the front and lateral views of the b) main composite structure and of the b) aluminium insert.

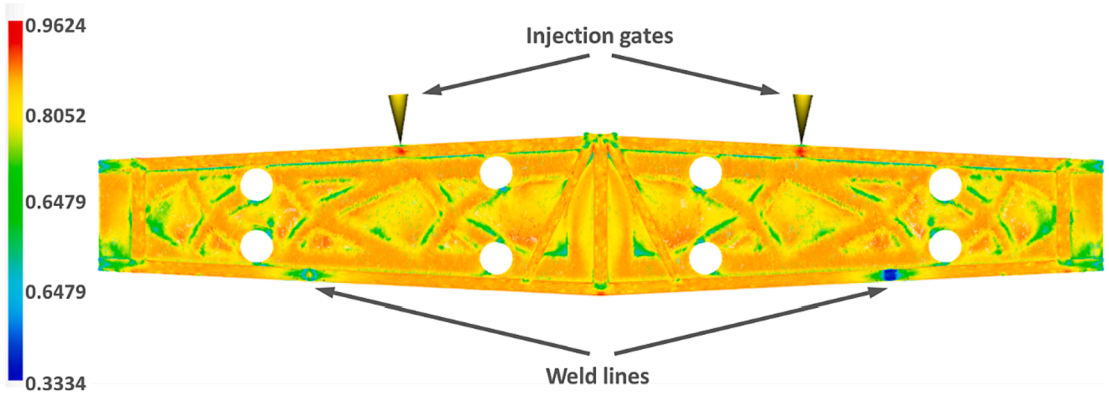

Fig. 4. Representation of the maximum eigenvalues of the fibre orientation tensor resulting from injection simulation of the demonstrator.

are associated to high alignment of the fibre along a preferential direction, while a random arrangement of the fibre in space is expressed by low values. Two weld-lines can be spotted in the lower flange areas, symmetrically located about the demonstrator's mid-span. Those regions result from the meeting of two flow fronts and are characterized by a mainly random fibre orientation. Finally, it is assessed that using the above-mentioned injection gates, a symmetrical FOD through the structure is provided. A non-symmetrical FOD would lead to uneven mechanical behaviour of the two halves of the demonstrator. The simulated fibre orientations were then used in the finite element modelling of the part.

2.2. Finite element modelling

A Finite Element Method (FEM) model of the PMH demonstrator was built in the Simulia Abaqus 2018 software (Dassault Sistèmes) [33] to simulate its static behaviour under the TBP test. The model accounts for the variability of the fibre orientation distribution induced by the injection moulding process and its effect on the properties of the SFRP by mapping the values of the fibre orientation tensor components obtained by process simulations onto the structural mesh (see previous section). Based on the local values of the fibre orientation tensor components, a macro-mechanical, non-linear behaviour of the composite material was obtained by a second order Mori-Tanaka homogenization scheme with J2 plasticity, as implemented in the Digimat software package [34]. No progressive damage or failure was modelled. A 3D strain-based Tsai-Hill

failure indicator was adopted.

Due to the symmetry of the demonstrator about its chassis-side vertical plane, the FEM model consisted in only one half of the structure, as shown in Fig. 5. Symmetric boundary conditions were applied on the chassis-side surface of the model. Two reference points were located and rigidly connected to the composite shell structure at the contact regions between the demonstrator and the loading/supporting edges of the TPB test set-up. A 10 mm downward displacement was imposed to the reference point at the loading edge along the y axis (see Fig. 5), while the downward displacement along the y axis and the rotation about the z axis (see Fig. 5) of the reference point at the supporting edge were prevented. The mesh used consisted of 2 mm average sized 10-node quadratic tetrahedral elements.

The mechanical behaviour of the 6061-T6 aluminium was described by a linear constitutive model up to yielding, then the power law:

$$\sigma_{pl} = K\varepsilon_{pl}^{n} \tag{1}$$

was used to model its strain hardening. Where K and n are the strength and strain hardening coefficients, respectively (reported in Table 1, from [35]). The mechanical behaviour of the short glass fibres was simulated by an isotropic linear elastic constitutive model, while that of the polyamide-66 (PA66) matrix was simulated by an isotropic elastoplastic constitutive model. The latter was based on the J2-plasticity model with the strain hardening described by the exponential and linear law:

$$\sigma_{pl} = Y\varepsilon_{pl} + \sigma_{\infty}[1 - e^{-m\varepsilon_{pl}}] \tag{2}$$

where Y is the linear hardening modulus, σ_{∞} and m are the saturation flow stress and exponent, respectively. Two constitutive material models were considered for the mechanical behaviour of the PA66: one for Dry As-Moulded (DAM) state at 23 °C and one for a conditioned state at 23 °C and 50 % relative humidity. A second order Mori-Tanaka homogenization scheme was applied to evaluate the mechanical properties of the homogenized composite. Failure Indicators (FI) of the composite were also provided by a 3D strain-based, transversally isotropic Tsai-Hill failure criterion, which reads:

$$\sqrt{FI} = \frac{\varepsilon_{11}^2}{X^2} - \frac{\varepsilon_{11}(\varepsilon_{22}+\varepsilon_{33})}{X^2} + \frac{\varepsilon_{22}^2+\varepsilon_{33}^2}{Y^2} + \left(\frac{1}{X^2} - \frac{2}{Y^2}\right)\varepsilon_{22}\varepsilon_{33} + \frac{\left((2\varepsilon_{12})^2 + (2\varepsilon_{13})^2\right)}{S^2} + \left(\frac{1}{Y^2} - \frac{1}{4X^2}\right)(2\varepsilon_{23})^2 \tag{3}$$

where X and Y are the maximum axial and in-plane tensile strains, respectively, while S is the maximum transverse shear strain. The values of X, Y and S, considered in the strain-based failure criterion for DAM and conditioned SGFR PA66 are reported in Table 2, respectively. The material modelling of the SGFR PA66 was carried out by mean field homogenization within Digimat-MF package of the Digimat suite by MSC Software [34]. All the relevant parameters used in modelling the behaviour of the 6061-T6 aluminium and the short glass fibre reinforced PA66 are reported in Table 1. The parameters used for the mean field homogenization of the SGFR PA66 were extracted from the calibrated material's card provided by the material's supplier for the Digimat MX package.

Table 1
Relevant parameters used for modelling the mechanical behaviour of each material.

Material	E [MPa]	K [MPa]	Y [MPa]	σ_{∞} [MPa]	n	m
6061-T6	68,900	376.5	–	–	0.05	–
Glass PA 66	72,000	–	–	–	–	–
DAM	2600	–	70	46	–	125
Cond	1300	–	50	36	–	85

Table 2
Parameters of the 3D strain-based, transversally isotropic Tsai-Hill failure criterion for DAM and conditioned SGFR PA66.

SGFR PA66	X	Y	S
DAM	0.028	0.033	0.19
Cond	0.038	0.041	0.3

The FOD within the composite main structure, resulting from the injection simulation, described in section 2.1, was considered in the numerical simulation of the PMH demonstrator. The results of the injection simulation were mapped on the FEM structural mesh using Digimat-MAP [34] software. This allows for the local anisotropic material properties, depending on the local FOD, to be evaluated and accounted for in the simulation.

2.3. Experimental

An extensive experimental campaign was performed to characterize the behaviour of the PMH demonstrator when subjected to a longitudinal load, simulating the typical force transmitted by the wheel to the control arm. Quasi-static, creep and impact tests were carried out to reproduce the loading scenarios that the suspension control arm normally faces during its working conditions.

2.3.1. Quasi-static test

Load controlled quasi-static tests were carried out on both the PMH and the polymeric demonstrators. This allows the different failure

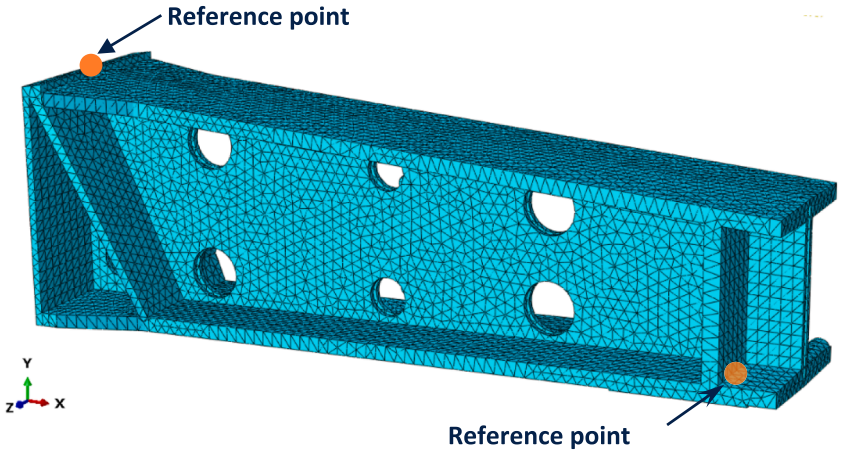

Fig. 5. FEM model of the PMH demonstrator. Reference points are highlighted.

behaviour of the two demonstrators' configurations to be assessed. The demonstrators were tested on an MTS Alliance RF/150 under a TPB set-up, with a test speed of 5 mm/min and a span between the supports of 265 mm. Mid-span deflection was measured by using an MTS 632.06H-30 displacement gage.

Three polymeric demonstrators were all tested in dry as-moulded conditions at room temperature, while the PMH demonstrators were split in two batches. The fifteen demonstrators belonging to the first batch were all tested in as-moulded conditions. Five samples were tested for each temperature level considered of −40 °C, 23 °C and 85 °C, as these are within the typical operating temperature range of automotive components. The five demonstrators of the second batch were tested inside a climatic room at a temperature of 23 °C and 50 % of relative humidity. Before testing, these latter demonstrators underwent conditioning to attain a moisture content, in equilibrium with the testing environment, of 0.9 %. Conditioning allows the moisture content effect on the stiffness of the composite main structure to be evaluated.

The bending stiffness of the demonstrator, k, was evaluated as the slope of its load–deflection curve by:

$$k = \frac{\Delta F}{\Delta \delta} \tag{4}$$

where the deflection interval, $\Delta\delta$, between 0.5 mm and 1 mm, and the corresponding load interval, ΔF, were considered. Within the considered load and deflection ranges, the static responses of the demonstrators were linear for any testing conditions.

2.3.2. Creep tests

Creep tests were performed to evaluate the possible effects of constant loads, combined with temperature ageing, with a consequent reduction of mechanical performance. Moreover, polymer structures often show a relaxation behaviour after the load application [36]. This could affect the correct assembly operations and, consequently, the working conditions. The effect of the applied load level and of the temperature was investigated. The tests were performed using the same TPB set-up mentioned above. Considering the number of the available demonstrators and the timing requested by a single test, in the experimental campaign one load level and two temperatures were evaluated for the polymeric demonstrator and two load levels and three different temperatures were evaluated for the PMH demonstrator, as shown in Table 3. The tests were carried out for a duration of 500 h focusing the attention on the primary and secondary creep phases [36] in the materials behaviour.

The creep tests were performed using a testing machine developed by the authors from the Politecnico di Torino [37]. The testing machine is shown in Fig. 6 and Fig. 7. To speed up the tests, the machine was designed to test two samples at the same time. During the whole test, the demonstrators are positioned inside a climatic chamber as shown in the Fig. 6 and Fig. 7. All the tests were performed at controlled temperature. The load is applied through a leverage system, and it is measured with a strain gauge load cell, whereas the deformation of the demonstrator is measured with a LVDT sensor.

2.3.3. Impact tests

Impact tests were performed to characterize the dynamic response of the demonstrator. The test configuration can be associated to a TPB test in dynamic condition. Fig. 8 shows the test set-up. The support was specifically designed to fit the demonstrator. It consists of two span supports leaning on a guideway screwed on a metal plate that is then fixed on the machine chamber's floor. The two supports are designed to slide on the guideway and adjust the span according to the test requirements. The span support has two vertical arms. On each arm two screws are inserted to hold the demonstrator during the impact test, avoiding undesired lateral movements of the demonstrator. For all the impact tests, the distance between the support spans was set to 265 mm.

The tests were performed using a CEAST Fractovis Plus free-fall drop dart testing machine. The impacting energy is adjustable by setting the falling height and the impacting mass. The dart had a cylindrical shape, with a hemispherical tip having a diameter of 12 mm. The dart impacted the demonstrator exactly at its central section.

A falling mass of 16 kg was used, and the falling height was set at different values for each impact test, in order to evaluate the demonstrator response when submitted to different levels of supplied energy E_0, in the range from 5 J to 20 J. A piezoelectric load cell was placed at the top extremity of the dart and the applied load signal was acquired at a frequency of 1 MHz. During the downward travel of the falling mass, some potential energy can be lost due to friction, thus requiring the energy balance to include the non-conservative term W_f, as illustrated in equation (2):

$$E_0 = mgh = \frac{1}{2}v_p^2 + W_f \rightarrow W_f = mgh - \frac{1}{2}v_p^2 \tag{5}$$

where m is the falling mass, g is the gravity constant, h is the initial falling height, v_p is the measured dart velocity at the impact and W_f is the non-conservative work due to friction. The dart velocity is measured by an electro-optical device (photocell). This device is used also to trigger the load acquisition.

The displacement of the dart during the impact is evaluated by the double time integration of the acceleration, retrieved by the Newton's law:

$$a(t) = g - \frac{F(t)}{m} \tag{6}$$

$$v(t) = \int_{t_0}^{t_f} a(t)dt + v_p \tag{7}$$

$$s(t) = \int_{t_0}^{t_f} v(t)dt \tag{8}$$

where $F(t)$ is the force signal acquired by the load cell, $a(t)$ is the acceleration time history of the dart, t_0 and t_f are respectively the first time instant of the impact and the time instant at which the load drops to zero, $v(t)$ and $s(t)$ are, respectively, the velocity and the displacement time history of the dart during the impact.

The energy E_{ab} absorbed by the demonstrator during the impact correspond to the area under the force–displacement curve:

$$E_{ab} = \int_{s_0}^{s_f} F(s)ds \tag{9}$$

where s_f and s_0 are the dart position evaluated respectively at t_f and t_0.

Table 3
Parameters considered for the creep tests.

Polymeric demonstrator		PMH demonstrator	
Temperature [°C]	Load [N]	Temperature [°C]	Load [N]
23	980	−10	980
50	–	23	1470
–	–	50	–

3. Results and discussion

3.1. Quasi-static tests and simulations

Fig. 9 shows the load–deflection curve resulting from quasi-static tests carried out on the polymeric and PMH demonstrators at room temperature in the DAM condition. Both structures displayed a linear initial response to the load. Then a progressive, although small, stiffness reduction made the structure responses slightly deviate from linearity up to failure. The PMH demonstrator resulted slightly stiffer (+16 %) than

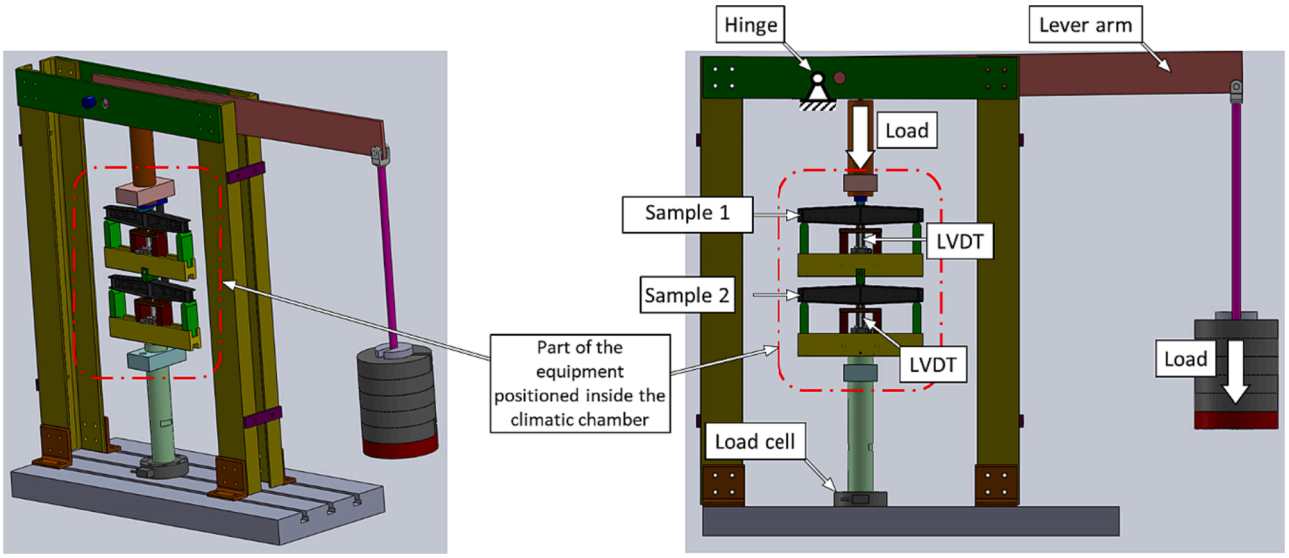

Fig. 6. Rendering of the creep testing machine and description of different components.

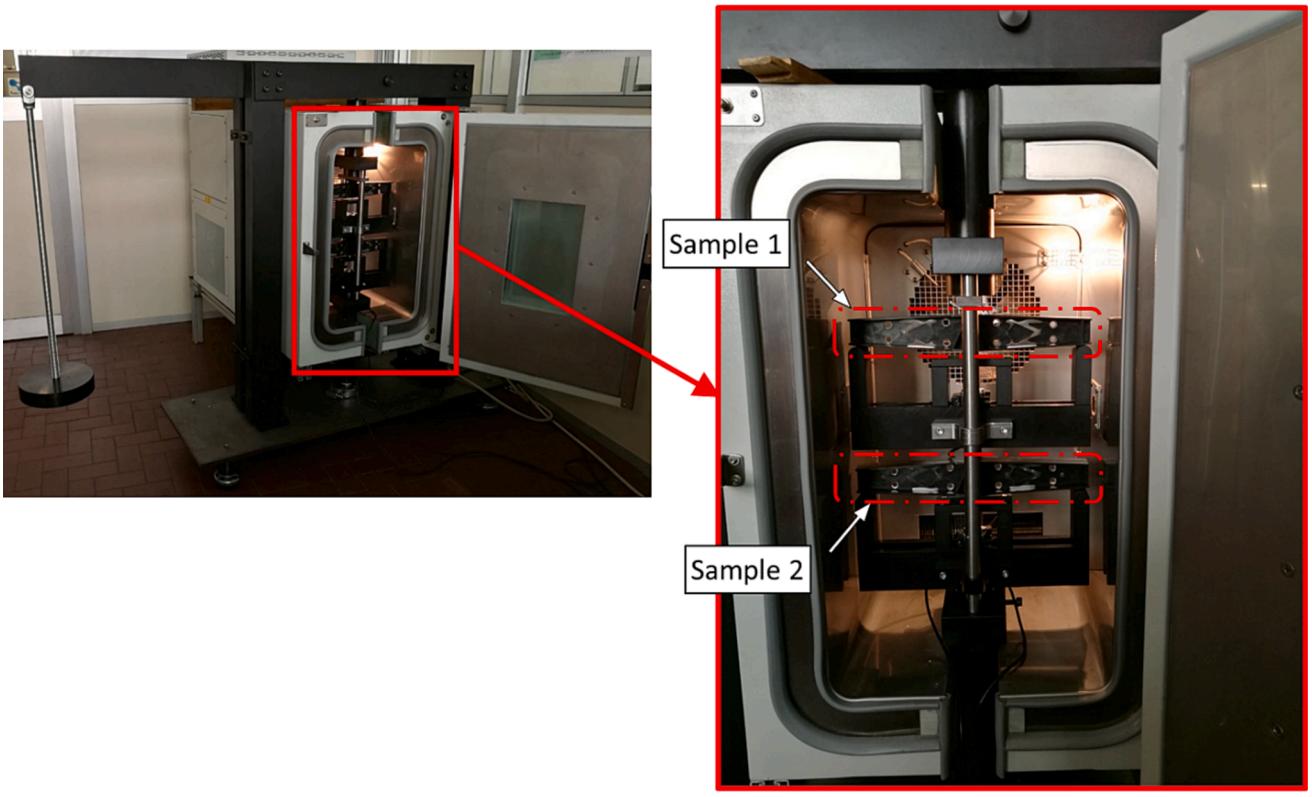

Fig. 7. Creep testing machine before test starting.

the polymeric one. Although the aluminium insert was meant only as a mean to prevent separation at failure, it contributed to the overall stiffness of the PMH demonstrator.

The polymeric demonstrators consistently failed at a load level of about 6.7 kN with a corresponding deflection of about 3.9 mm. A catastrophic and brittle failure was observed, resulting in the complete separation of the structure in two halves at midspan, as shown in Fig. 10. a. In all the polymeric demonstrators the crack onset was located on the lower flange at the end of the oblique reinforcement rib. This was the targeted location for the failure to occur. Then the crack suddenly propagated throughout the structure on a path that follows the oblique reinforcing rib.

On the other hand, the PMH demonstrators failed with larger scatter of maximum loads and corresponding deflections. This could be attributed to the non-uniform bonding between the metal insert and the polymeric structure, resulting from the manufacturing process. The adhesion between the polymer and the metal was not a parameter considered in this work. A proper surface treatment of the metal insert, aimed at enhancing the surface wettability and adhesion with the polymeric materials, could be considered in future developments of this work.

Moreover, it is likely that the load transfer between the polymeric

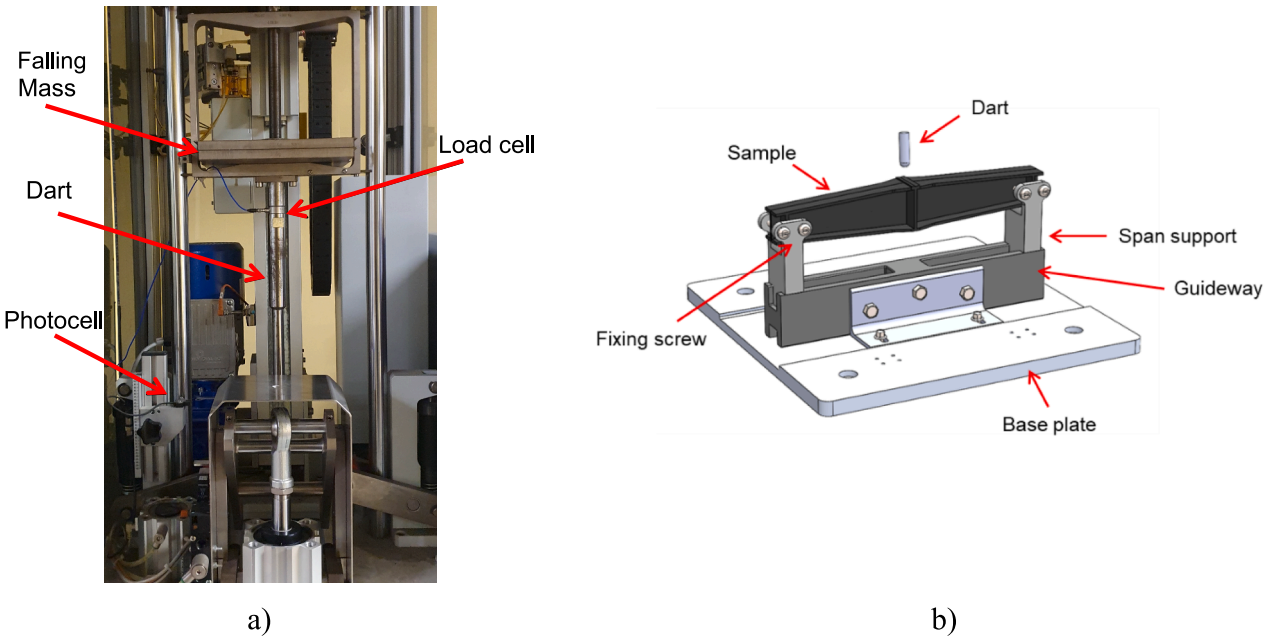

Fig. 8. Impact test set-up, a) drop dart testing machine; b) demonstrator support.

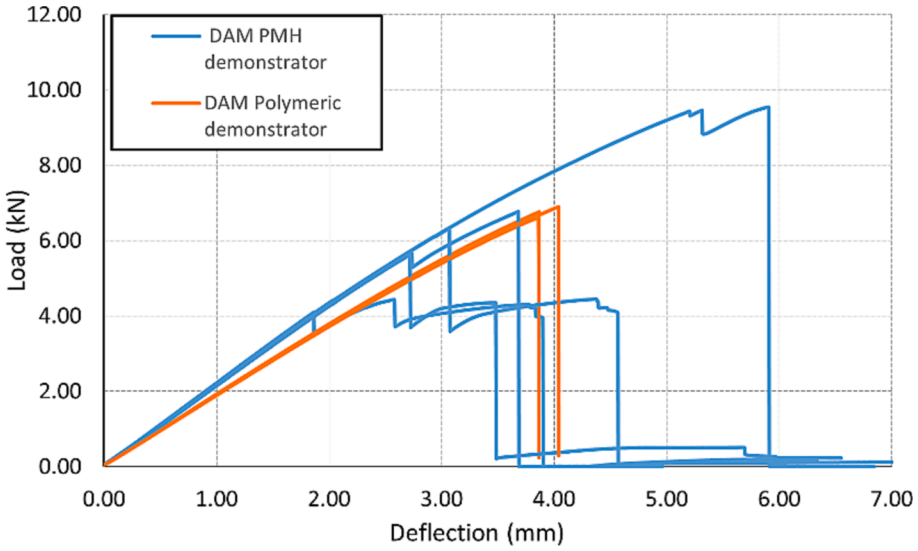

Fig. 9. Load-deflection curves of the PMH and polymeric demonstrators tested in dry as-moulded condition at room temperature.

and the metallic parts was mainly achieved by mechanical interlock of the reinforced polymer flowing into the cavities of the metal insert. In any case, the first load drop of the load–deflection curves of the PMH demonstrators (Fig. 9) did not correspond to a total loss of load carrying capability of the structure. Indeed, final failure occurs at a later stage, as shown in Fig. 9.

The failure event was characterized by two subsequent phases: the first failure of the composite main structure, which is related to the first load drop of the force–deflection curves of Fig. 9, was followed by the partial failure of the metallic insert, which caused the ultimate load drop of the aforementioned curves. The order of the events is inferred by the lower strain at break of the polymer than that of the aluminium, provided that at the moment of the first load drop, the metal and the polymer reached the same local strain value. The load carrying ability of the PMH demonstrator did not drop to zero when the composite main structure failed, opposite to the polymeric demonstrators, which underwent full separation. After the first load drop, a further increase of the load can be observed for the PMH demonstrators, presumably due to the load transfer to the aluminium insert.

A picture of a failed PMH demonstrator is reported in Fig. 10.b. It is worth noting that the failure of the composite main structure consistently originated close to one of the weld-lines (see Fig. 4). The crack suddenly propagated through the structure but always stopped before crossing it entirely from the bottom to the upper flange. The crack stop is due to the transfer of the load to the aluminium insert, which deformed plastically before its partial failure. It is important to highlight that the presence of the insert always avoided the complete separation of the structure. At the fracture location, the metal insert appeared as fully debonded from the polymer. This confirms that load transfer was mainly achieved by mechanical interlock. Whether an improved adhesion between the polymer and the metal insert could improve the overall performance or not should be investigated. Particularly, it would be interesting to check if an improved adhesion might even prevent the metal insert to undergo large strains, which are fundamental for the

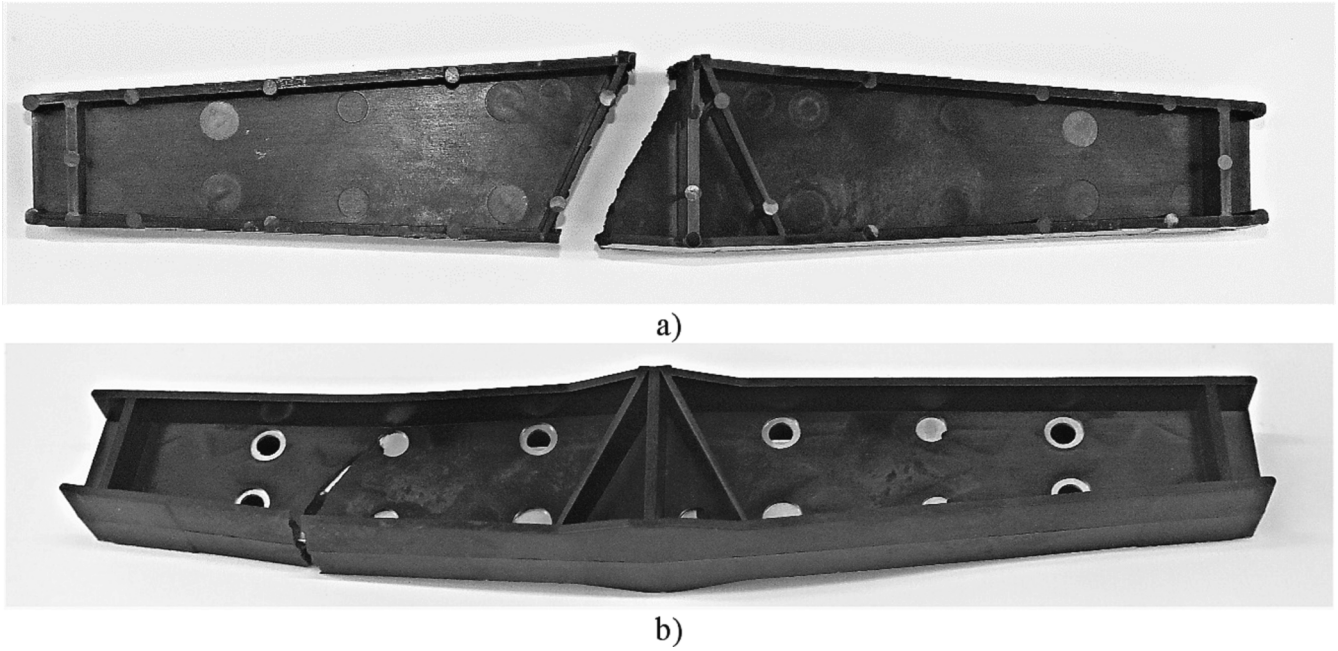

Fig. 10. Comparison of the failure mode of a) Polymeric, b) PMH demonstrators.

avoidance of full separation.

The average values of initial stiffness, maximum load and deflection at failure, along with their standard deviation, of the DAM polymeric and PMH demonstrators are reported in Table 4.

Fig. 11 showcases a comparison between the quasi-static behaviour of the DAM and of the conditioned PMH demonstrators (also including the simulated load–displacement curves). As expected, the tested conditioned demonstrators displayed a more compliant behaviour with respect to their as-moulded counterparts. Their quasi-static response is characterized by a more extended plastic region before failure. Both features are due to the plasticizing effect brought by the water on the polymeric matrix of the composite main structure. The failure mechanism of the conditioned PMH demonstrator is similar to that of their dry-as-moulded counterparts, as evidenced by the trend of the load–deflection curves of Fig. 11. Despite the consistency of the initial stiffness of the conditioned PMH demonstrators, they also fail for a large scatter of loads and deflections. Their failure load is comparable to that of their as moulded counterpart, instead, the deflections at failure are larger.

Fig. 11 shows good agreement between the simulated and the experimentally obtained quasi-static behaviour of the PMH demonstrator in DAM condition. The numerical simulation however tends to slightly overestimate the stiffness and the overall response of the demonstrator. Conversely, despite a low overestimation of the initial stiffness, the numerical simulation largely overestimates the overall quasi-static behaviour of the "conditioned" demonstrator.

In the numerical simulation the FI of each mesh element is computed by locally applying the strain-based Tsai-Hill criterion reported in equation (3). The element failure condition is reached when its FI approaches one. However, the numerical simulations did not include the deletion of elements whose FI was greater than one. Therefore, from an analysis of the FI of the mesh elements two conditions were identified as indicators for the failure of the polymer part of the PMH demonstrators: when the FI of the first mesh element is equal to 1, and when all the elements through the thickness at the most critical location exceed 1, respectively. The triangular and square points on the simulated load–deflection curves of the DAM and conditioned demonstrators, reported in Fig. 11, identify the first and second damaging conditions, respectively.

For both the DAM and conditioned PMH demonstrators, the first critical element which experience a FI greater than one is found near the hole of the aluminium insert closest to the supporting edge, as shown in Fig. 12. Similarly, for both the DAM and conditioned demonstrators, the critical area where the FI of all the elements through the thickness of the polymer part exceed one is found close to the first critical element, as shown in Fig. 13.

The location of the failure predicted by the simulations does not correspond with the experimental one, which was at the weld-lines. However, within the numerical simulations the strength reduction at the weld lines regions was not modelled. For a short glass fibre reinforced polyamide, Medda and Fisa [38] reported a weld-line strength that is close to that of the matrix, irrespectively of the fibre fraction, whereas the overall strength reduction of tensile tested specimens, due to weld-lines, ranged from 40 % to 55 %. Therefore, the strength of the composite shell at the weld-lines was most probably overestimated.

Moreover, perfect adhesion between the composite shell and the aluminium insert was assumed in the structural simulation. This

Table 4
Average values of initial stiffness, maximum load and deflection at failure of the polymeric and PMH demonstrators both tested and simulated. Standard deviations are reported in brackets.

Demonstrators Tested	Simulated	Stiffness [kN/mm]	Maximum load [kN]	Deflection at failure [mm]
Dry As Moulded				
Polymeric at 23 °C		1.892 (±0.021)	6.757 (±0.144)	3.922(±0.116)
PMH at 23 °C		2.187 (±0.048)	6.532 (±2.924)	3.473(±1.841)
PMH at – 40 °C		2.304 (±0.065)	6.283 (±1.556)	2.901(±0.840)
PMH at 85 °C		1.270 (±0.018)	5.621 (±0.482)	9.679 (±0.964)
	PMH at 23 °C	2.381	10.1	5.25
Conditioned				
PMH at 23 °C		1.659 (±0.037)	6.783 (±0.862)	6.392(±1.957)
	PMH at 23 °C	1.878	8.2	5.95

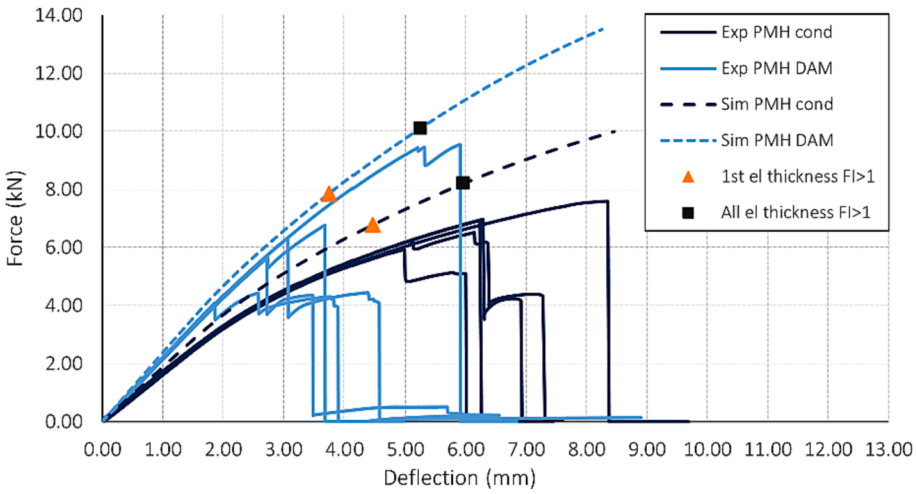

Fig. 11. Comparison between the simulated and experimentally obtained load–deflection curves of the dry as-moulded and conditioned PMH demonstrators.

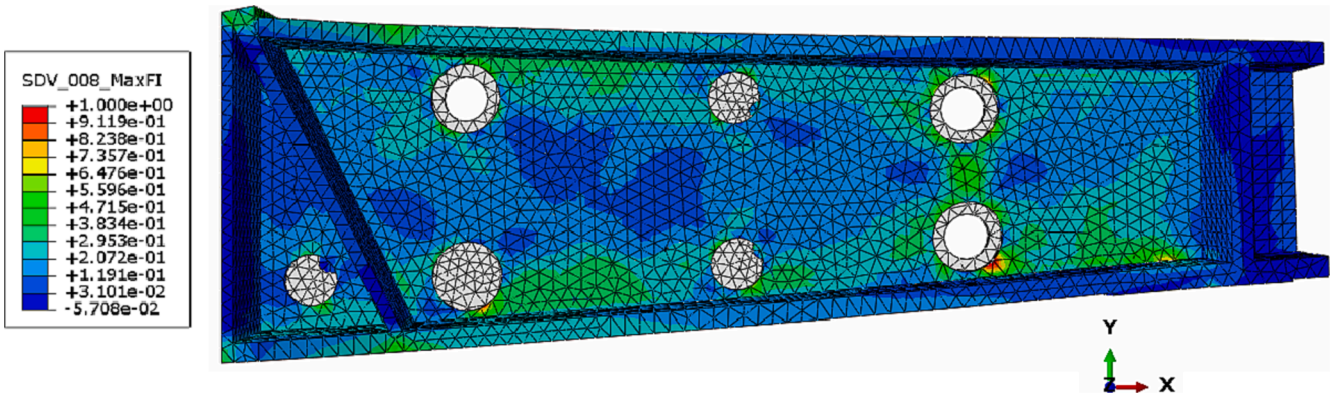

Fig. 12. FI contour map of the mesh elements of the PMH demonstrator when first element in the thickness of the composite structure is greater than one.

prevented the effects of the composite-metal debonding on the demonstrator's strength to be considered. Therefore, although the agreement between the simulated and experimental curves, on which the design of the demonstrator was based, is fairly good, the effect of weld-lines and the adhesion between the polymer and the metal remain open issues in the modelling of this PMH demonstrator. The comparison between tests and simulations suggests that these points should be addressed first, e.g. like in [39], before attempting to improve the material's model of the reinforced polyamide using more advanced methods like [40,41].

The response of the PMH demonstrator to the quasi-static load at different testing temperature is shown in Fig. 14. At all testing temperatures, the load–deflection curves show the first load drop typical of the composite structure failure, and a load recovery region where the aluminium insert carries the load. The complete separation of the PMH demonstrator was thus prevented at any investigated temperatures.

The demonstrators tested at − 40 °C showed a linear response up to failure, even if a quite large scatter of the failure load is observed, ranging from 5.2 to 7.8 kN. They failed for low deflection level that is about 3 mm. Conversely, the demonstrators tested at 85 °C displayed a small elastic region and an extended plastic behaviour. Their failure occurred at higher deflections, about 10 mm, under a load in the range from 5 to 6 kN. The initial stiffness, the maximum load and deflection at failure of the PMH demonstrators tested at different temperatures are reported in Table 4.

The failure of all the quasi-static tested PMH demonstrator occurred at the flow weld-lines (Fig. 10.b), regardless of the testing temperature or their moisture content. It is well known that the weld-lines are indeed the weakest region of a structure [38]. Under the TPB test set-up used, the lower flange area of the demonstrator is highly loaded. The stress acting in the flow weld regions likely exceeds the local strength in those critical regions. Therefore, the crack which develops there caused the failure of the PMH demonstrators. It is then suggested to carefully design the injection process in order to move the location of the flow weld-lines away from critical loaded regions. Martulli et al. [42] reported the detrimental effect of the weld surfaces on the strength of an automotive component. Moving their location from high stressed to low stressed regions led to a beneficial effect on the strength of the component. Moreover, weld-lines could also become points of initiation of fatigue cracks. The fatigue behaviour of this type of structure needs to be addressed in future works.

3.2. Creep tests

The results of the creep tests are shown in Fig. 15 in terms of vertical displacement of the cross section as a function of the time for the PMH demonstrators where the load applied is maintained constant. For both types of demonstrators, the temperature is the most influencing parameter. Considering the polymeric demonstrators (Fig. 15a), the primary creep and the slope of the secondary creep are more pronounced at the lower temperature and for the lower load level. The opposite behaviour was obtained considering the PMH demonstrators (Fig. 15b), where the behaviour was affected by the presence of the metal insert. In any case, the higher the temperature, the higher the displacement, being the creep behaviour of the structure governed by the creep of the polymer, in this range of temperature. Comparing the creep curves at 980 N and 50 °C of the polymeric demonstrators

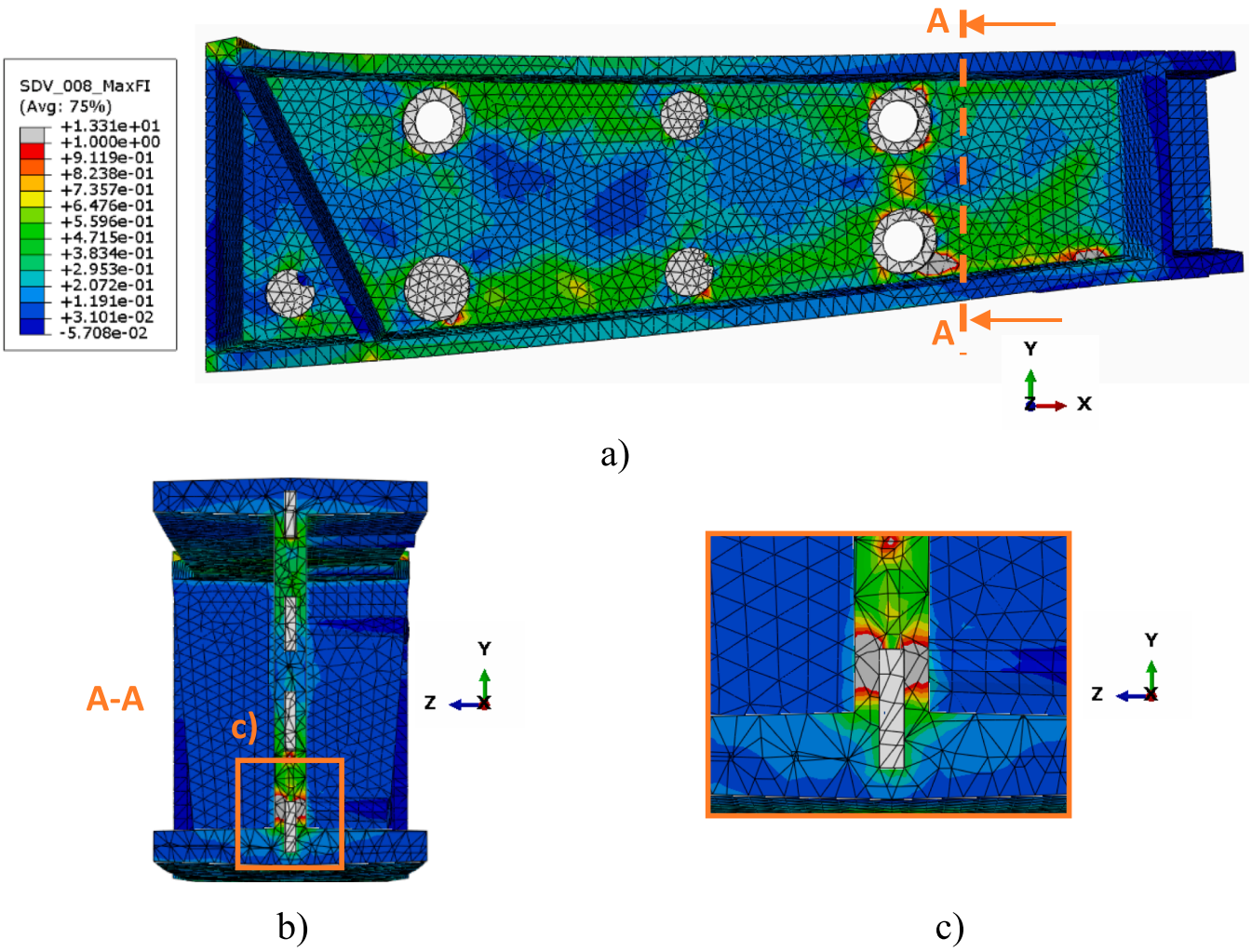

Fig. 13. a) FI contour map of the mesh elements of the PMH demonstrator when all the elements in the thickness of the composite structure is greater than one. b) cut view of the demonstrator failed section c) detail of b).

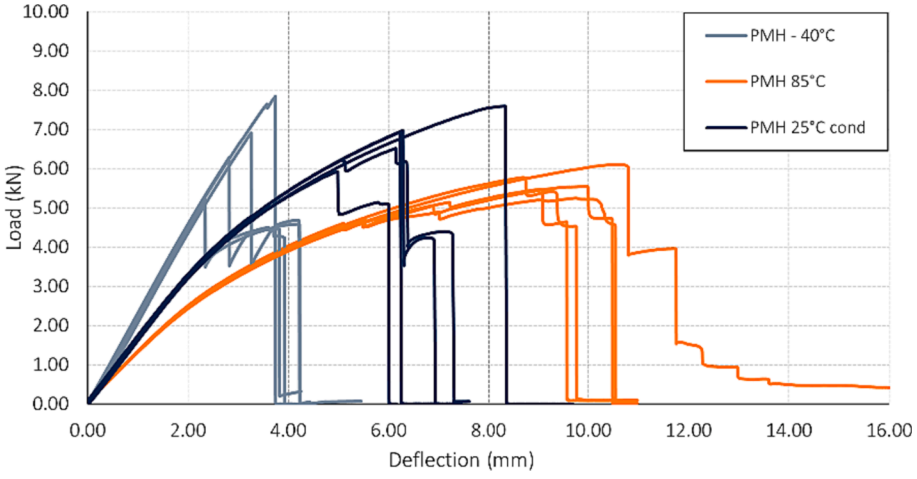

Fig. 14. Load-deflection curves of the PMH demonstrators at different testing temperatures.

(Fig. 15a) and of the PMH ones (Fig. 15c), it can be concluded that the presence of the metal insert considerably reduces the creep displacement. It is likely that the creep of the polymer causes a load transfer to the metal insert, which is not prone to creep in the considered range of temperatures. The samples were not tested until failure, however it can be reasonably assumed that the metal insert would be capable of preventing separation, as it was demonstrated by the quasi-static tests. Furthermore, in the PMH version, the heterogeneity of the materials can lead to residual stresses due to the different thermal expansion coefficients of the constituents, which could relax over time. This aspect

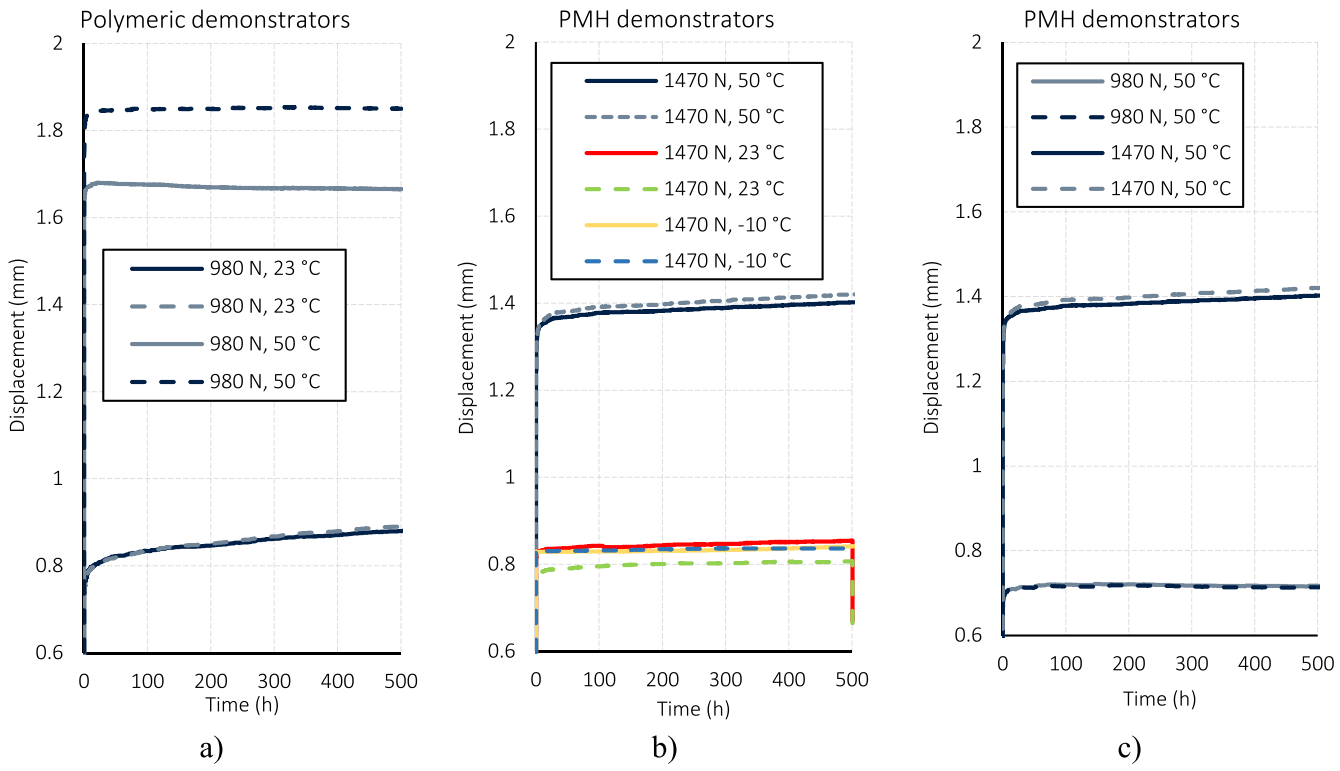

Fig. 15. Results of the creep tests in terms of vertical displacement of the demonstrator as a function of the time: a) polymeric demonstrators; b) PMH demonstrators, effect of temperature with fixed applied load; c) PMH demonstrators: effect of load at 50 °C.

could be the subject of further investigations.

3.3. Impact tests

Fig. 16 shows the results of the impact tests carried out at different energy levels in terms of force vs dart displacement. Due to the high acquisition frequency and the high dynamics of the test, a lowpass filter with a cut off frequency equal to 1600 Hz was used to smooth the oscillations of the force signal. The tests were conducted across a range of energy from 5 J to 20 J and multiple repetitions were performed for each energy level. However, to simplify and enhance the interpretation, the results presented pertain to the impact tests performed at E_0 of 5 J, 10 J, 15 J, and 20 J. The bending stiffness of the demonstrator appears to be not affected by the value of E_0: the slopes until the maximum force are well superimposed for all the curves, thus no remarkable strain-rate effects are evidenced. The maximum load carried by the demonstrator increases of about 1kN every 5 J of provided energy, at least for the 5, 10 and 15 J tests. Fig. 17 shows the energy versus dart displacement plot. Here, the total energy stored in the demonstrator E_{max} is the maximum of each curve, whereas the internally absorbed energy E_{ab} is represented by the upper intersection of the considered energy curve with the vertical line corresponding to the abscissa value equal to the final dart displacement. The difference between E_{max} and E_{ab} is the elastic energy E_{el} returned to the dart. However, in the case of the 20 J test, a failure of

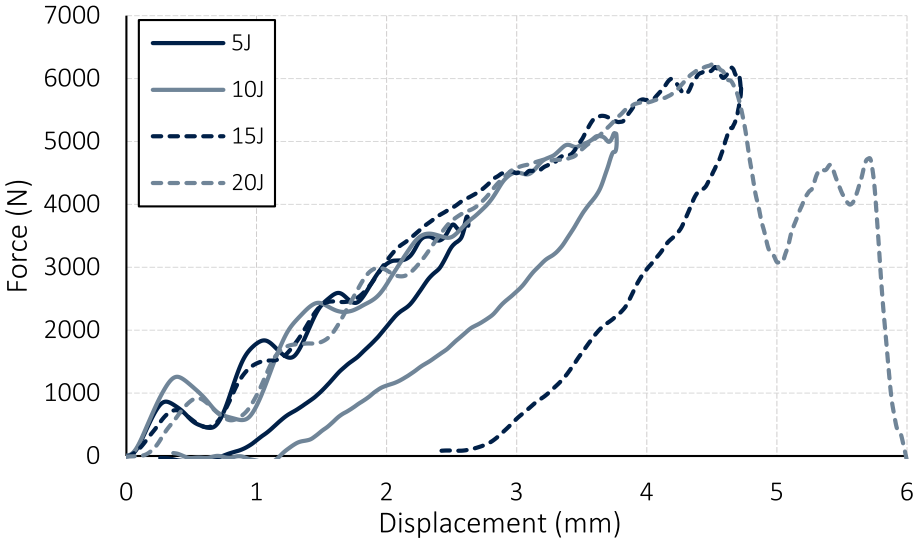

Fig. 16. Force – dart displacement plot for the demonstrators tested at 5, 10, 15 and 20 J of supplied energy.

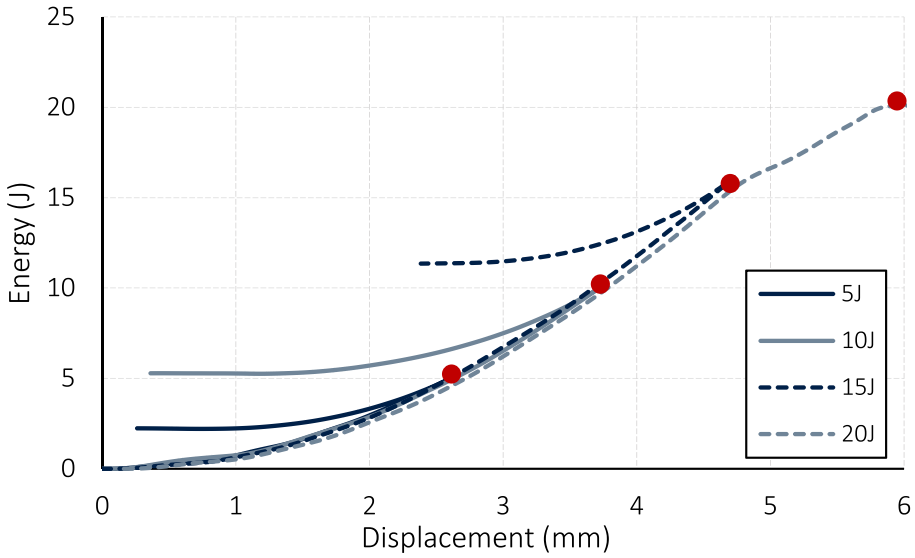

Fig. 17. Energy – dart displacement plot for the demonstrators tested at 5, 10, 15 and 20 J of supplied energy. The red symbols indicate E_{max}.

the structure took place after the load peak and no dart rebound occurred. The impact energy in this case is completely dissipated and the E_{el} returned to the dart is null. The resulting relevant values are reported in Table 5 for the tested demonstrators.

Considering the curve at 5 J of impact energy of Fig. 16, the maximum force carried by the demonstrator was 3974 N corresponding to a dart displacement of 2.7 mm. A residual deformation of 0.74 mm implies that an amount of energy was absorbed via plastic deformation or fracture. The absorbed energy is well readable in the energy vs displacement plot (Fig. 17). In this case, the absorbed energy was equal to 2.24 J. This energy includes the energy absorbed by the inelastic deformation of the polymeric material, the energy dissipated by friction due to contact and sliding of the dart on the demonstrator, the energy absorbed by the plastic deformation of the metal insert, and the fracture energy of the lateral plastic ribs, as shown in Fig. 18b. Similar considerations hold for the demonstrator subjected to an E_0 equal to 10 J. As can be seen from Fig. 16, the 10 J curve maintains roughly the same shape and proportions as the 5 J curve: the maximum force carried by the demonstrator was about 5030 N corresponding to a dart displacement of 3.7 mm. Its residual deformation was 1.2 mm corresponding to an E_{ab} of 5.28 J. The fractures, appreciable by a visual inspection, were similar to the previous case (Fig. 18.b). At 15 J of supplied energy, the maximum force was about 6181 N with a maximum displacement of 4.7 mm. The shape of the force–displacement curve (Fig. 16) is more splayed with respect to the previous two cases. A higher amount of energy was absorbed by the fracture that originated and propagated from the lower flange up to the side face of the demonstrator (Fig. 18.c). The metallic insert did not fracture. However, it is plausible that it absorbed energy by plastic deformation, due to the high residual displacement of the demonstrator after the impact (about 2.5 mm). A further increase in the supplied energy E_0 led to the failure of the demonstrator. The crack trigger point was always in correspondence of one of the flow weld-lines in the lower flange (Fig. 18.b), like in the quasi-static tests. The fracture propagated also inside the metal insert (Fig. 18.d). Despite this, the complete separation of the structure never occurred. It is worth to notice that both for E_0 equal to 15 and 20 J, the maximum force was around 6000 N. This can be considered as the maximum load carrying capability of the demonstrator in impact condition.

Table 5
Results of the impact tests in term of energy indicators and maximum force.

E_0 (J)	Force Peak (N)	E_{ab} (J)	E_{el} (J)	Failure Location	Metallic insert
5	3974	2.24	2.76	Rib	Not Failed
10	5030	5.28	4.72	Rib	Not Failed
15	6181	11.35	4.65	Diffused	Not Failed
20	6238	20.09	–	Diffused	Failed

Belingardi et al [43] defined the damage degree, η, as the ratio of the energy absorbed E_{ab} to the maximum energy E_{max} that the demonstrator can store (as elastic and plastic deformation, fracture, and fragmentation). Another important consideration regarding the damage assessment can be done by looking at the energy level at maximum load E_{blm}. This represents the amount of energy transferred to the demonstrator before the main failure occurs. The β value is defined as the ratio between E_{blm} to the critical energy, E_{crit}, whose definition is explained in the following. These damage assessment indexes are plotted in Fig. 19.a.

Fig. 19.b shows the Energy Profile (EP) diagram: the absorbed energy E_{ab} is plotted as a function of the supplied energy E_0. The 45° inclined Equal Energy Line (EEL) represents the ideal condition in which all the E_0 is completely converted in E_{ab}. This is not the typical case where the absorbed energy is less than the impact energy. When the supplied energy is totally absorbed by the demonstrator, we identify the critical energy value E_{crit} and, consequently, the Critical Line (CL), reported in orange in Fig. 19.b for sake of exemplification The region on the left of the critical line (CL) is called subcritical region. In this region, the impact energy does not generate the global failure of the structure and all the tested points lie below the EEL. The green vertical segment obtained from the intersection between a tested point and the EEL gives the E_{el}. In the supercritical region, on the right of the CL line, the energy provided leads the demonstrator to fail and completely lose its load bearing capability. In this region, the red vertical segment, obtained from the intersection between a tested point and the EEL, represents the excess energy that the demonstrator was not capable to absorb, that is transferred and dissipated by the machine dumpers.

At the lower energy levels (i.e. 5–10 J) the damage index η is relatively small and remains between 0.4 and 0.5: the demonstrator preserves its global structural integrity, and it is capable to store and then elastically release at least half of the supplied energy. The other half is dissipated by several concurring mechanisms: internal material damping, plastic deformation of the polymer and metal inserts, composite fracture in correspondence of the weld-lines regions and friction between the dart and the demonstrator (Fig. 18.b). Increasing the E_0 to 15 J the damage index increases to 0.7: the demonstrator is still capable of release elastic energy, even if a higher amount of energy is dissipated by the polymer fracture (Fig. 18.c). The transition energy (E_{crit}) between the

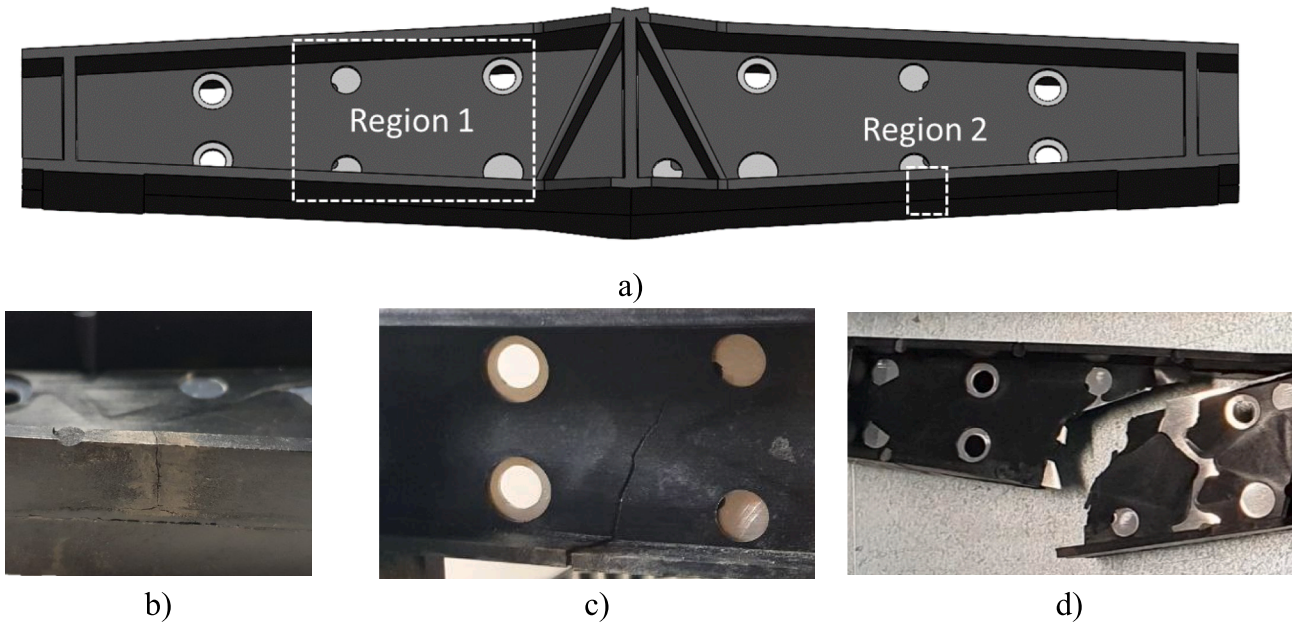

Fig. 18. Overview of the fracture modes. A) CAD model of the specimen and reference fracture regions; b) rib fracture in the region 2 at 5 and 10 J of supplied energy; c) polymer fracture in the region 1 at 15 J of supplied energy; d) polymer and metal insert fracture in the region 1 at 20 J of supplied energy.

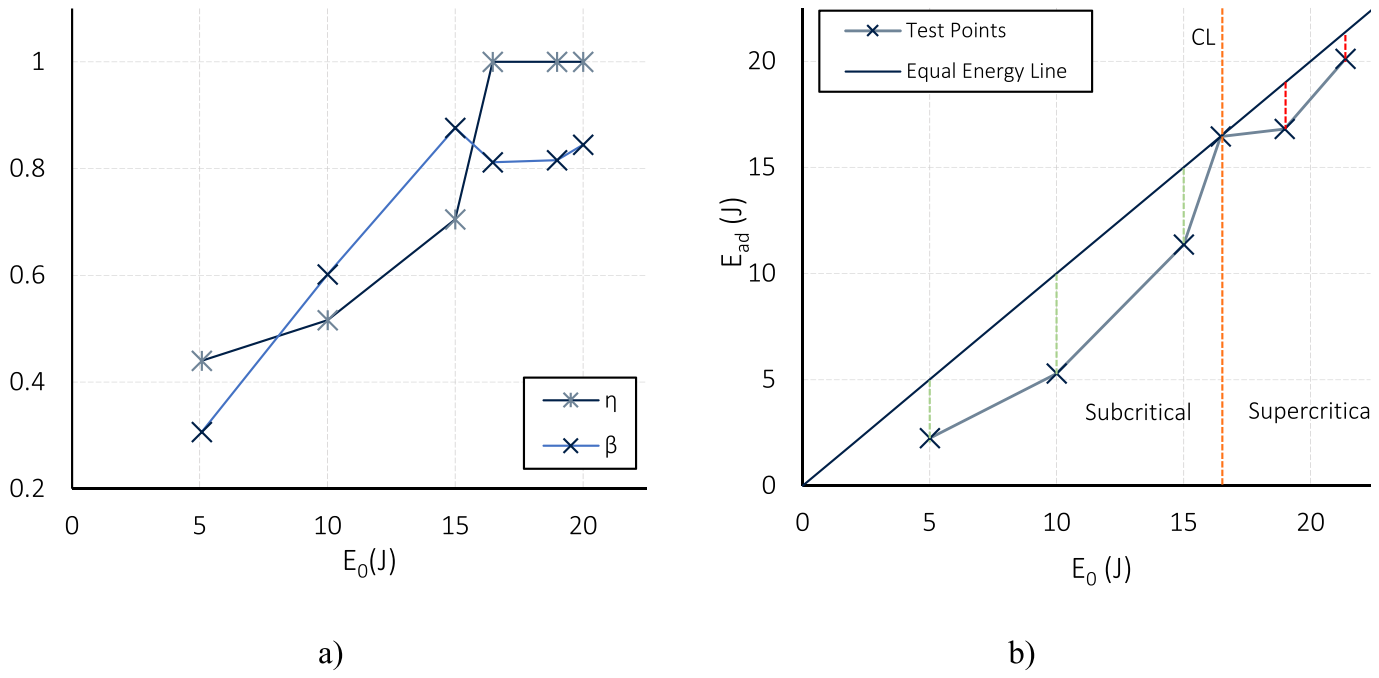

Fig. 19. a) Damage assessment indices as a function of E_0; b) energy profile plot as a function of E_0.

subcritical and supercritical behaviour was estimated to be around 16.5 J. This value was determined by testing several samples with energies ranging from 15 to 20 J, in order to precisely define the energy threshold for the transition from subcritical to supercritical behaviour. The damage index is equal to 1, meaning that no elastic energy is released back by the demonstrator. In Fig. 19.b, it is worth noting that the tested point at this energy level is lying on the EEL: all the supplied energy E_0 is absorbed or dissipated by the demonstrator by fracture and deformation. The damage index remains constant to 1 for further increase of E_0 and the tested points fall in the supercritical region. For these test points, the maximum load remains about 6000 N. This value can be interpreted as the maximum load carrying capability of the structure in impact condition and it is close to the quasi-static one. It is worth to notice that for an E_0 equal or greater than 15 J, the β index is between 0.8 and 0.9. This means that, independently from the E_0, the energy at which the onset of the main failure occurs (i.e. E_{blm}) is equal to the 80–90 % of the critical energy.

4. Conclusions

The present work presents a feasibility study on a car's suspension control arm based on PMH technology. A simplified demonstrator of the

component's critically loaded region was devised in two versions: an all-composite version, made of SGFR PA66, and a PMH version, in which an aluminium insert was embodied in the SGFR PA66 main structure. Both versions were manufactured via injection moulding. In the PMH version, the short fibres composite was over-moulded on to the aluminium insert.

The PMH solution was specifically designed such that only the composite main structure carries the applied load. The metal insert only delivers the explicit function of ensuring the residual integrity of the PMH demonstrator after failure of the composite main structure.

Quasi-static, creep and impact test were performed on the demonstrators under a TBP set up to simulate the everyday operating conditions of a suspension control arm. Test results evidenced a well reproducible behaviour of the PMH demonstrator under any testing conditions. However, the variability of the adhesion between the metal insert and the polymeric structure yields the PMH demonstrators to fail in quasi-static tests with large scatter of loads and deflections.

Creep tests showed that the presence of the insert reduces the deformation of the polymeric insert under prolonged static loads, especially at high temperature (50 °C). The temperature, however, largely affect the deformation of both the demonstrator versions.

Impact tests confirmed the independency of the PMH demonstrator stiffness upon the impact energy. The structural integrity of the demonstrator is maintained up to a maximum impact energy of 15 J. However, at this energy the fracture of the lower flanges occurs leading to non-negligible values of residual deformation (2.5 mm). In any case, complete separation is avoided by the metal insert.

In almost all the failure events of the PMH demonstrator, the flow weld-lines triggered the onset of the crack, regardless of the applied loading type. Therefore, considering the injection moulding of a real component, the unavoidable weld-lines should be confined in non-critical areas, particularly to avoid the risk of initiating fatigue cracks. The analysis of the fatigue strength of this demonstrator constitutes a possible future development.

A catastrophic failure was observed for the polymeric demonstrators, resulting in the complete separation of the structure in two halves. Instead, in the PMH version, no separation of the PMH structure was always guaranteed by the metal insert after the failure of the composite main structure. Considering these results, this work supports the feasibility of a novel short fibre reinforced PMH solution for automotive safety relevant components, like the suspension control arms, where the composite part is the main load bearing one and the metal part is used only to prevent separation. Nevertheless, to fully demonstrate the feasibility of such PMH structure, the following main limitations of the present work should be overcome in future works: more advanced modelling techniques (progressive damage, role of weld-lines, fatigue, temperature and strain rate effects, adhesion between the metal and the polymer), more testing, like fatigue tests at different temperatures, and improvement of the adhesion between the polymer and the metal.

CRediT authorship contribution statement

A. Canegrati: Formal analysis, Validation, Visualization, Writing – original draft. **A. Bernasconi:** Conceptualization, Writing – review & editing. **L.M. Martulli:** Formal analysis, Writing – review & editing. **P. Barriga:** Investigation, Formal analysis. **G. Previati:** Formal analysis. **D. Fiumarella:** Formal analysis, Investigation. **A. Scattina:** Conceptualization, Writing – review & editing. **E. Spini:** Resources. **G. Belingardi:** Supervision, Writing – review & editing. **G. Mastinu:** Supervision.

Declaration of competing interest

The authors declare that they have no known competing financial interests or personal relationships that could have appeared to influence the work reported in this paper.

Data availability

Data will be made available on request.

Acknowledgements

The authors gratefully acknowledge Regione Lombardia and EU for funding project SOLE2, project ID 141072, POR 2014-2020 FESR / Innovazione e Competitività, and the project partners Barnem Tecnologie Plastiche S.r.l. and Metal Stampi di Maccarinelli e Cucchi S.r.l. for the manufacturing of the components and of the mould, respectively. The authors from Politecnico di Milano acknowledge support by the Italian Ministry for Education, University and Research through the project Department of Excellence LIS4.0 (Integrated Laboratory for Lightweight e Smart Structures).

The raw/processed data required to reproduce these findings cannot be shared at this time as the data also forms part of an ongoing study.

References

[1] Cecchel S. Materials and technologies for lightweighting of structureal parts for automotive applications: a review. SAE Int J Mater Manuf 2021;14(1):81–97.
[2] Messana A, Sisca L, Ferraris A, Airale A, Carello M. Lightweight design of a multi-material suspension lower control arm,“ in *ASME 2020 International Design Engineering Technical Conferences and Computers and Information in Engineering Conference*, Virtual, Online, August 17-19, 2020.
[3] Carello M, De Carvalho Pinheiro H, Messana A, Freedman A, et al. Composite control arm design: a comprehensive workflow. SAE Technical Paper 2021–01-0364 2021. https://doi.org/10.4271/2021-01-0364.
[4] Anandakumar P, Timmaraju MV, Velmurugan R. Development of efficient short/continuous fiber thermoplastic composite automobile suspension upper control arm. Mater Today: Proc 2021;39(4):1187–91.
[5] Kim DH, Choi DH, Kim HS. Design optimization of a carbon fiber reinforced composite automotive lower arm. Compos Part B: Eng 2014;58:400–7.
[6] Carello M., Airale A.G., “Composite suspension arm optimization for the city vehicle XAM 2.0”. In: Öchsner A., Altenbach H., “Design and Computation of Modern Engineering Materials. Advanced Structured Materials”, Springer,54,2014 10.1007/978-3-319-07383-5_18.
[7] Banks AJ. Composite Lightweight Automotive Suspension System (CLASS). SAE Technical Paper 2019–01-1122 2019.
[8] Feraboli P, Gasco F, Wade B, Maier S, Kwan R, Masini A, et al., “Lamborghini ”forged composites(R)“ technology for the suspension arms of the Sesto Elemento,” in *26th ASC technical conference*, Montreal, 2011.
[9] Czél G, Jalalvand M, Wisnom MR. Design and characterisation of advanced pseudo-ductile unidirectional thin-ply carbon/epoxy–glass/epoxy hybrid composites. Compos Struct 2016;143:362–70. https://doi.org/10.1016/j.compstruct.2016.02.010.
[10] Eksi S, Genel K. Bending response of hybrid composite tubular beams. Thin-Walled Struct 2013;73:329–36.
[11] Eksi S, Kapti AO, Genel K. Buckling behavior of fiber reinforced plastic-metal hybrid-composite beam. Mater Des 2013;49:130–8.
[12] Wang Z, Jin X, Li Q, Sun G. On crashworthiness design of hybrid metal-composite structures. Int J Mech Sci 2020;171:105380.
[13] Zhu G, Sun G, Yu H, Li S, Li Q. Energy absorption of metal, composite and metal/composite hybrid structures under oblique crushing loading. Int J Mech Sci 2018;135:458–83.
[14] Schweizer S, Becker-Staines A, Troster T. Separation and reclamation of automotive hybrid structures made of metal and fibre-reinforced plastic. Waste Manag 2020;115:74–82.
[15] Khalid Muhammad Yasir, Arif Zia Ullah, Ahmed Waqas, Arshad Hassan. Recent trends in recycling and reusing techniques of different plastic polymers and their composite materials. Sustain Mater Technol, 31, 2022. 10.1016/j.susmat.2021.e00382.
[16] Zoellner OJ, Evans JA. “Plastic-Metal Hybrid- A new development in the injection molding technology,” in *ANTEC*. San Francisco: CA, USA; 2002.
[17] Grujicic M, Sellappan V, Arakere G, Sevr N, Erdmann M. Computational feasibility analysis of direct-adhesion polymer-to-metal hybrid technology for load-bearing body-in-white structural components. J Mater Process Technol 2008;195(1–3):282–98.
[18] Grujicic M, Sellappan V, Omar M, Sevr N, Obieglo A, Erdmann M, et al. An overview of the polymer-to-metal direct-adhesion hybrid technologies for load-bearing automotive components. J Mater Process Technol 2008;197(1–3):363–73.
[19] Grujicic M, Sellappan V, Pandurangan B, Li G, Vahidi A, Sevr N, et al. Computational analysis of injection-molding residual-stress development in direct-adhesion polymer-to-metal hybrid body-in-white components. J Mater Process Technol 2008;203(1–3):19–36.
[20] Grujicic M, Sellappan V, Kotrika S, Arakere G, Obieglo A, Erdmann M, et al. Suitability analysis of a polymer–metal hybrid technology based on high-strength steels and direct polymer-to-metal adhesion for use in load-bearing automotive body-in-white applications. J Mater Process Technol 2009;209(4):1877–90.

[21] Li L, Sun L, Dai Z, Xiong Z, Huang B, Zhang Y. Experimental investigation on mechanical properties and failure mechanisms of polymer composite-metal hybrid materials processed by direct injection-molding adhesion method. J Mater Process Technol 2019;263:385–95.
[22] Vasconcelos RL, et al. Injection overmolding of polymer-metal hybrid structures: A review. Polym En Sci 2023;63(3):691–772.
[23] https://techcenter.lanxess.com/scp/americas/en/docguard/TI_2006-47_US_Case_D_BKV30_Faurecia_-_Frontend_TT.pdf?docId=9042806.
[24] Meurer E. Plastic/metal hybrid technology in automotive front ends. SAE Technical Paper 1999–01-3243 1999.
[25] Lorenzo L, Naughton P. Structural front-end carrier using long glass fiber polypropylene. SAE Technical Paper 2002–01-3563 2002.
[26] Naughton P, Rottger J, Bowser B. A new approach to hybrid front end systems. SAE Technical Paper 2002–01-1229 2002.
[27] Fonseca JH, Han G, Quagliato L, Kim Y, Choi J, Keum T, et al. Design and numerical evaluation of recycled-carbon-fiber-reinforced polymer/metal hybrid engine cradle concepts. Int J Mech Sci 2019;163:105115.
[28] Fonseca JH, Quagliato L, Yun S, et al. Preliminary design of an injection-molded recycled-carbon fiber–reinforced plastic/metal hybrid automotive structure via combined optimization techniques. Struct Multidisc Optim 2021;64:2773–88.
[29] Fonseca JH, Jang W, Han D, Kim N, Lee H. Strength and manufacturability enhancement of a composite automotive component via an integrated finite element/artificial neural network multi-objective optimization approach. Compos Struct 2024;327:117694.
[30] Sun G, Yu H, Wang Z, Xiao Z, Li Q. Energy absorption mechanics and design optimization of CFRP/aluminium hybrid structures for transverse loading. Int J Mech Sci 2019;150:767–78.
[31] https://knowledge.autodesk.com/support/moldflow-insight/learn-explore/caas/CloudHelp/cloudhelp/2019/ENU/MoldflowInsight-Reference/files/GUID-86ACC406-0FB9-4E7A-950F-EFAB610C39E7-htm.html.
[32] Advani SG, Tucker IC. The use of tensors to describe and predict fiber orientation in short fiber composites. J Rheology 1987;31:751–84.
[33] Dassault Systemes, Abaqus v2018 manual, 2018.
[34] SMC Software Belgium SA, Digimat User Manual, 2018.
[35] H. Kuhn, D. Medlin, ASM Handbook Volume 8 Mechanical Testing and Evaluation. s.l.:ASM International, 2000.
[36] Raghavan J, Meshii M. Creep of polymer composites. Compos Sci Technol 1997;57:1673–88.
[37] Scattina A, Roncato D, Belingardi G, Martino G. Investigation of creep phenomenon on composite material for bolt connections. Compos Struct 2015;134:378–83.
[38] Meddad A, Fisa B. Weldline strength in glass fiber reinforced polyamide 66. Polym Eng Sci 1995;35(11):893–901.
[39] Pan W, Sun L, Mu A, Lv W. Interface constitutive modeling and failure propagation mechanisms of integrated polymer-metal hybrid (PMH) structures. Compos Struct 2023;306:116593.
[40] Xu H, Kuczynska M, Schafet N, Welschinger F, Hohe J. Modeling the anisotropic temperature-dependent viscoplastic deformation behavior of short fiber reinforced thermoplastics. Compos Sci Technol 2021;213:108958.
[41] Dean A, Reinoso J, Jha NK, Mahdi E, Rolfes R. A phase field approach for ductile fracture of short fibre reinforced composites. Theor Appl Fract Mech 2020;106:102495.
[42] Martulli LM, Creemers T, Schöberl E, Hale N, Kerschbaum M, Lomov SV, et al. A thick-walled sheet moulding compound automotive component: Manufacturing and performance. Compos A 2020;128.
[43] Belingardi V. Low velocity impact tests of laminate glass-fiber-epoxy matrix composite material plates. Int J Impact Eng 2002;27(2):213–29.